circle of Willis [1]. Under the effect of a single or a combination of factors, the arterial wall is progressively thinned and ballooned out to create an aneurysm. Recognized cofactors contributing to intracranial aneurysm growth and risk of rupture are for example hypertension, atherosclerosis, smoking, excessive alcohol consumption and oral contraceptives. Increased risk exists among patients presenting hereditary deficiencies such as hereditary polycystic kidney disease, Ehlers–Danlos syndrome, Marfan syndrome, fibromuscular dysplasia or family history of aneurysm disease [2–4], and between 7 to 20% of people who underwent an aneurismal rupture have a relative of first or second degree with a cerebral aneurysm diagnosed [5]. All this indicates that the biology and the resulting life cycle of a specific aneurysm is potentially influenced by a number of factors and coincidences, what allows for comparing the disease with a complex systems, where the variable factors want to be weighed and integrated according to their possibly varying role along the different periods of the aneurysm life cycle, i.e. initiation, growth and rupture.

Clinical studies reveal a prevalence of around 2% of the Western population having a cerebral aneurysm with a rupture incidence of only about 10 of 100,000 people per year [6]. Aneurysm rupture in these 10 people present mainly under the form of a subarachnoid hemorrhage (SAH), what results in high morbidity and mortality rates for the patients concerned [7], and this even under good medical care conditions. SAH conditions due to a ruptured aneurysm result for obvious reasons in high treatment cost. Treatment of unruptured cerebral aneurysm provides better results and at lower cost, however, not free of risk. With current diagnostic medical imaging methods, revealing increasingly such unruptured aneurysms as an incidental imaging finding, it seems of interest to search for criteria and methods that would allow for optimizing the rupture risk assessment and to weigh such risk against the risk of a potential treatment. To take into account the changing treatment risk, the assessment should be adjustable to the evolving treatment methods and standards. Such an educated approach may allow for reducing the stress conveyed to patients and may provide a useful support to the discussion and decision taking, while avoiding unnecessary treatment or supporting the decision on when and how to treat.

As outlined above, the multiple factors influencing the fate of a cerebral aneurysm require the use of a risk assessment model that perceives the condition as complex. Considering the roles of the different parameters in such a complex system, among others, the group representing biomechanical aspects is of special interest, because methods as developed in engineering and industry could be applied. Measurements or calculations of biomechanical factors include the intra-aneurismal blood flow, the mechanical load on the arterial wall and the peri-aneurismal environment in case appropriate boundary conditions can be defined. The aneurismal shape reflects the wall quality and is the resultant of the aneurysm evolution, and depends from the physiological load, as well as from the contact with surrounding tissues [8], very much alike the riverbed, represents the resultant of the river and the land it runs through. Rupture mainly results from the progressive degeneration and weakening of the three arterial wall constituents, the elastin fibers, the vascular smooth muscles and the collagen fibers. The last to go is the collagen network, which constitutes the major structural element of the aneurismal wall. Contrary to the mainly flow driven degeneration, there have been observation of morphological changes associated with aneurysm wall remodeling representing inflammation or repair attempts.

Through biology, all these mechanisms are influencing the aneurysm wall quality and therefore one could imagine addressing the disease and its evolution by pharmacological therapy influencing degeneration, inflammation or repair [9]. Although yet to explore further, in our view the most promising method to alter the biology of the aneurysm wall is acting on the fluid mechanic parameters, such as blood pressure, flow rates and patterns that may all, individually or in combination, alter the biological response of the wall constituents or of the endothelium, which in turn releases bioactive substances regulating the metabolism and matrix turnover of the aneurismal wall [1]. If acting on the vessel lumen side to implement flow correction through medical devices like coils and stents seems increasingly feasible, acting on the outside of the aneurysm wall is less promising. Modification of the peri-aneurismal environment is currently only possible by applying surgical wrapping methods [10].

Therefore blood flow modulation may constitute and increase its role as an efficient treatment principle, aiming either disconnection from the parent artery flow or restoration of a physiological flow in the parent artery. Neurosurgical treatment performed by placing a metallic clip around the aneurismal neck is closing definitively the aneurismal flow and may change the geometry of the parent artery. This could be seen as a therapy inducing flow modification in the aneurysm and the parent arteries. Although the surgical modality offers the advantage of a direct vessel repair, this is achieved with the effort of an open head surgery associated accordingly with patient discomfort and operative risk [7]. Less discomfort and procedural risk exists with endovascular repair, working minimally invasive through a small arterial puncture site and by using image guided treatment methods [11]. Endovascular treatment methods act by flow modulation in the aneurismal cavity or in the parent vessel. The aneurismal cavity can be filled with coils leading rapidly to aneurismal thrombosis once enough coils have been introduced. Use of stents may act as a scaffold to help keeping coils in an aneurismal cavity in case there is a large aneurysm neck and offering a higher vessel reconstruction success rate, with the stent acting as a scaffold for the vessel wall remodeling. The main difficulties of endovascular treatment are related to difficult access to the target area, intra-operative rupture risk and mainly a currently high peri-operative thromboembolic potential. Based on these facts, the decision for invasive treatment has to balance between the risks of treatment and the risks of natural disease course [12,13].

With this potential in mind, it is believed that stents alone will be able to redirect the flow in the parent artery and slow down the aneurismal flow leading to a thrombus formation, stabilizing the aneurysm without the need to enter and to touch the fragile aneurismal cavity. Prediction of intra-aneurismal flow alterations after stent placement could be helpful to foresee the effect and to allow for choosing the most adequate stent capable of inducing alone or together

Please cite this article in press as: Augsburger L, et al. Methodologies to assess blood flow in cerebral aneurysms: Current state of research and perspectives. J Neuroradiol (2009), doi:10.1016/j.neurad.2009.03.001

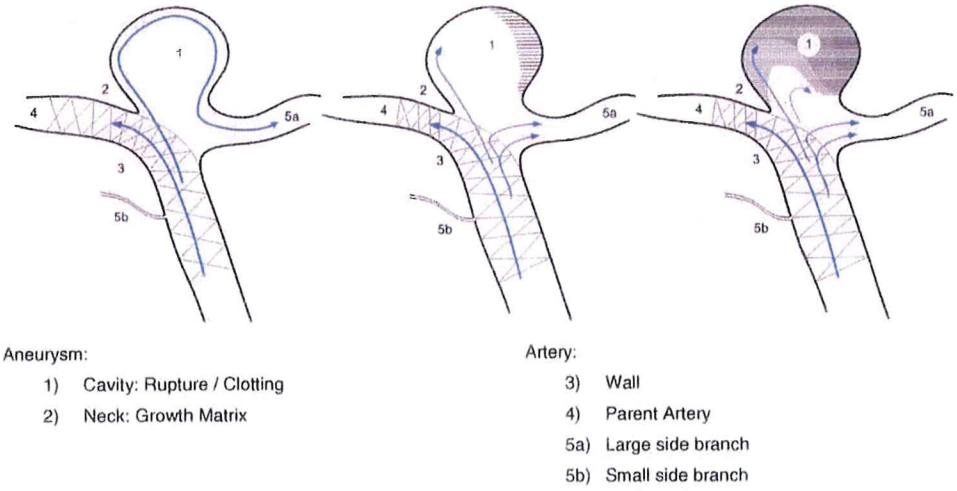

Figure 1 Illustration of the progression of clot formation in a bifurcation aneurysm model treated with an intracranial stent as seen in medical procedures.

with additional intra-aneurismal flow modifiers (coils) a stable and safe clot formation (Fig. 1).

Such predictions could empower medical doctors to choose the most appropriate treatment. Medical imaging companies would have to integrate numerical simulation tools and medical device companies would have to develop and produce improved endovascular prostheses — processes that are currently well under way.

In this paper, we present a review of the current state of research involving in vitro experiments and numerical simulations of intra-aneurismal flow in presence of a stent.

Experimental methods developed to assess blood flow changes due to a stent in intracranial aneurysms: evolution of methods and transparent in vitro vascular models (phantoms, replicas)

One of the objectives of experimental methods is to assess blood flow changes in aneurysms induced by flow diverters such as may be produced by a stent deployed in the parent artery. Assessing the device effect on flow in in vitro vascular phantoms is done to estimate in vivo flow effects to be expected. This effort is aimed mainly at predicting the chance to obtain thrombus formation within an aneurysm after stent placement. The tests may include assessment of effects on flow in the parent artery and its branches. There are quantifiable flow effects, such as values of velocities and pressure and their related parameters, including vorticity (circulation), helicity (rotation), wall shear stress (WSS), and oscillatory shear index among others. Visualization and classification of altered blood flow patterns appears further of interest when it comes to estimating stent efficiency.

The materials of vascular replicas have evolved and spatial resolution of 3D data improved stepwise, giving today possibilities to a range of model production reaching from simple idealized shapes up to complex, patient-specific cerebral aneurysm replicas based on three-dimensional rotational angiography (3D-RA) [14]. Using rapid prototyping (RP) technologies, 3D description of the aneurysm geometry serves to produce models made of transparent materials such as plexiglas (polymethyl-methacrylate), silicone or poly-vinyl-alcohol-hydrogel, (PVA-H). All such models are transparent and compatible with current medical imaging methods. Most used in our practice are silicone and PVA models. The low friction characteristics of PVA-H models and its elasticity close to soft tissue when compared to silicone models allow for more realistic simulation when it comes to study pulsatile flow effects.

The following flow measuring and visualization techniques have allowed for simple visualization up to a detailed mapping of the parameters defining flow within an aneurismal cavity.

Slip stream visualization

Slip stream visualization without device

In 1992, flow patterns around human cervical carotid bifurcations were visualized using digital subtraction angiography by injecting contrast agents [15], allowing for direct visualization of flow. The authors hypothesized that high WSS could cause degenerative changes in the endothelial layer, initiating the formation of saccular and fusiform intracranial aneurysms. One year later, by injection of fluorescent particles in the blood stream, Nakatani et al. could visualize spiral blood flows in vivo, both proximal and distal to arterial bifurcations located at the base of rat brains [16]. This study led to hypothesize on aneurysms development, growth, and rupture. Chong et al. compared the flow patterns in a vertebrobasilar artery model using slip stream visualization and MR based flow measurements. Flow profiles were found to be consistent between both techniques [17].

Slip stream visualization with device

Lieber et al. visualized the pulsatile flow patterns in an experimental flow apparatus using a laser-induced

Please cite this article in press as: Augsburger L, et al. Methodologies to assess blood flow in cerebral aneurysms: Current state of research and perspectives. J Neuroradiol (2009), doi:10.1016/j.neurad.2009.03.001

fluorescence of rhodamine dye. Various stents exhibiting four different porosities (comprised between 76 and 85%) were investigated and the results showed the difference of aneurismal vortex reduction in large and small arteries [18]. Using a photochromic dye, Rhee et al. visualized the flow in sidewall and in fusiform aneurysms models, and velocity and WSS changes due to various stents could be calculated. The results reported in these two studies revealed different results with flow reduction being not similar in both kind of models and with stents of various porosities, a less porous stent reducing the intra-aneurismal fluid motion significantly, and in the other, with stent porosity of less significant effect [19].

Particle illumination photography

Barath et al. studied 20 different stents of various ranges of porosity, permeability and filament diameter and quantified the reduction of the vortex displacement in two different neck-sized sidewall aneurysm models under unsteady flow conditions. Flow patterns were visualized by using glass particles and laser sheet translumination. The method defines a vortex center path line method obtained by sequentially subtracting each image taken, followed by identification of the vortex center and by tracking the vortex center producing a center path line. The conditions were studied without and in presence of different stents [20]. The authors raised the question of stent positioning effects. In a second study [21], the authors studied the intra-saccular flow pattern changes and the vortex velocity reduction induced by a stent in a internal carotid artery model retrieved from human vascular casting.

Particle image velocimetry (PIV)

PIV is a non-intrusive technique which allows reconstructing the velocity vectors fields in a flowing fluid seeded with particles. This technique, which is widely adopted in a variety of liquid and gas flows, has been used by Lieber et al. to quantify the effects of the strut size of three helical stents on flow [22], and by Canton et al. to measure the intra-aneurysm flow dynamics and mechanical stresses changes resulting from the placement of neuroform stents in bifurcating intracranial aneurysms models [23]. Measurements of the circulation demonstrated a reduction of the vortex magnitude due to the placement of one, two or three stents. PIV was also used by Yu et al. in sidewall aneurysm models under steady flow conditions, where the Reynolds number varied from 200 to 1600. They noticed that for Reynolds number higher than 700, a large recirculating vortex would be formed. The insertion of two different stents damped the flow movement, the mean velocity and reduced consequently the WSS [24].

Laser Doppler velocimetry (LDV)

Other techniques, such as LDV are also used to assess flow and WSS in patient-specific geometries. LDV is an accepted method in velocity measurement investigations based on the cross of two beams of collimated, monochromatic, and coherent laser light in the flow of the fluid being measured.

Validation and comparison with numerical simulations and clinical data without device. Liou et al. compared tridimensional flow fields with computational fluids dynamics (CFD) simulations in idealized, lateral and rigid cerebral aneurysm models and found that the inflow angle into the lateral aneurysm, the maximum WSS acting on the distal lip of the lateral aneurysm and the intra-aneurismal vortical motion increased with decreasing aneurysm size, underlining the potential critical aneurysm geometrical configuration leading to rupture [25]. Tateshima et al. measured and evaluated the alternation and distribution of WSS in two aneurysm models (middle cerebral artery and basilar tip, both with blebs at their domes). They noticed that both aneurysm models blebs were exposed to high WSS, region where the arterial wall is the finest in vivo [26]. Hollnagel et al. used LDV to validate phase-contrast magnetic resonance angiography (PC-MRA) in a patient specific aneurysm model under steady flow conditions. They found only minor differences in velocity field distribution and mean velocity values between both techniques, the accuracy depending on the artery size and the measurement plane positioning [27].

Our group measured the aneurismal flow, qualified and quantified the flow reduction due to the insertion of an endovascular prosthesis using PIV. Fig. 2A to D present the aneurysm flow in a lateral aneurysm placed on a curved parent artery model without (A and C) and with (B and D) a commercial stent (Neuroform II, Boston Scientific, Fremont, CA) under a steady flow of 100 ml/min. The corresponding Reynolds number is 70.2 and the stent effective porosity defined to be the ratio of the free surface area over the stent area is calculated to reach 82%. For this specific case, we quantified the mean velocity magnitude reduction within the aneurysm to reach 69%; in other words, only 31% of the flow is remaining; 78% reduction in vorticity.

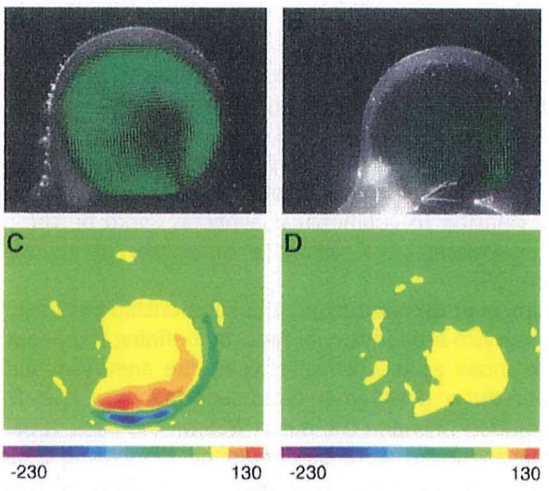

Figure 2 Velocity vector fields without (A) and with a stent (B); vorticity magnitudes without (C) and with stent (D) are presented.

Please cite this article in press as: Augsburger L, et al. Methodologies to assess blood flow in cerebral aneurysms: Current state of research and perspectives. J Neuroradiol (2009), doi:10.1016/j.neurad.2009.03.001

Prediction of hemodynamical changes due to a stent in aneurysms models using computational fluids dynamics: numerical models

Simulation without stent

With the improvement of computer power and the evolution in computational fluid dynamics, numerical simulations gained in speed and precision. Nowadays, an up-to-date laptop or small cluster of computers has enough power to compute the flow in a patient specific aneurismal geometry under unsteady flow conditions within a few hours. The quality of medical images permits the reproduction of the cerebral geometry very precisely, so that intra-aneurismal flow can be simulated accurately. The combination of advanced image processing and geometrical modeling techniques with computational fluid dynamics enhanced the generation of detailed hemodynamical aneurismal flow in patient-specific geometries [14,28]. Cebral et al. developed a CFD pipeline allowing for the computation of the arterial and aneurismal flow based on CTA and 3D rotational angiography image data. The morphological boundaries of the vessel lumen were obtained through 3D reconstruction, segmentation and meshing. Physiological flow boundaries were set based on ultrasound measurements. Subsequent computation provided blood flow patterns, WSS, oscillatory shear and pressure data. Their results enhanced the understanding of intra-aneurismal flow patterns and their relation to aneurismal rupture risk [29]. Four flow pattern categories were defined: simple stable, complex stable, simple unstable and complex unstable. Aneurysms of the first group were less at risk of rupture whereas aneurysms presenting a complex unstable flow were more likely to be associated with rupture. The additional evaluation of the jet type entering into the aneurismal cavity showed it to be a potential indicator of aneurismal rupture. Indeed, geometries aiding the creation of a fluid jet impinging on a small aneurismal wall area belonged mainly to ruptured groups. Conversely, geometries where flow was more diffused and entered less canalized into the aneurysms were less at risk of rupture [30].

Some studies used such CFD simulations to propose flow-based indices for the prediction of aneurismal rupture risk or even the rupture location [31,32]. It has been shown that flow features are strongly dependant on aneurysm geometry. It has been further hypothesized that flow, having a strong relation to geometrical aspects, could be the principal equivalent of a surrogate biomarker of aneurismal rupture [29].

Valencia et al. pointed out the relationship between WSS and aneurysm area index. In fact, by defining the aneurysm surface index as the ratio between the aneurysm surface area and the arterial lumen cross-sectional area, they found a correlation between the mean WSS on the aneurismal sac and the aneurysm surface. Aneurysms presenting a higher surface with low mean WSS were more likely to rupture [33]. Numerical simulations matched to clinical observation allowed to correlate the high fluid-induced WSS with ruptured areas [34].

Simulation with stent

Due to complex problem of representing a patient-specific geometry and due to the huge computational load numerical simulations are requiring, blood flow was simulated in two-dimensional idealized geometries. Ohta et al. investigated the hemodynamical flow patterns in intracranial aneurysms bifurcations models before and after stent placement over a cardiac cycle. As blood was modeled to be a non-Newtonian fluid, the lowered values of peak velocities and WSS due to stent placement allowed to localize the region of increased dynamic viscosity [35].

Numerical simulations were also performed to assess how stents can be optimized to enhance their ability at diverting the flow and, consequently, reduce the risk of rupture. Stent effects on aneurismal flow, WSS, pressure and oscillatory shear were quantified. Aenis et al. [36] investigated the flow patterns in a sidewall aneurysm under physiological pressure and flow conditions. The stent altered the local hemodynamics and substantial differences in flow patterns and pressure values were observed and quantified. Stuhne et al. developed mesh generation tools to manage the difficulties encountered with the meshing of stented aneurysm geometries. More detailed flow patterns description could be provided [37]. Cebral et al. present an adaptive grid embedding technique to manage the mesh difficulties due to scales differences between artery and stent strut sizes [38]. The modeling of stent deployment in a patient-specific geometry is currently achieved by morphing technique. Appanaboyina et al. developed a method that deforms a straight stent model and fits it in a patient-specific geometry. Basically, a cylindrical surface composed of shell elements is generated along the skeleton of the parent vessel of the patient-specific geometry and is considered as an elastic material. This surface is expanded under the action of internal smoothing forces and external attractive forces to the wall. The resulted deformation of the cylindrical surface is performed interactively and the expansion is stopped when most of the points on the cylinder touch the wall [39]. This methodology is successfully used to model patient-specific anatomies with different stents allowing for the exploration of different stent designs efficiency.

Other numerical simulation techniques, such as Lattice–Boltzmann method (LBM), were developed to avoid the mesh generation difficulties encountered with finite element and finite volume methods [40]. An LBM-based clotting model for stented intracranial aneurysms has been developed [41] and a direct clotting metric measuring the percentage of clotting of aneurysm impacted by different stents have been compared with indirect metrics measuring both velocity and WSS reductions inside the aneurysm [42].

Our group measured the aneurismal flow, qualified and quantified the flow reduction due to the insertion of an endovascular prosthesis using the techniques described above. Fig. 3 shows the results of blood flow simulation in a patient specific geometry under unsteady flow conditions. The aneurysm geometry was retrieved using 3D-RA and the volume was processed to be finally meshed. Blood flow was measured in the internal carotid artery of a healthy volunteer using PC-MR technique [43]. This physiological flow waveform was applied at the inlet by defining fully spatial

Please cite this article in press as: Augsburger L, et al. Methodologies to assess blood flow in cerebral aneurysms: Current state of research and perspectives. J Neuroradiol (2009), doi:10.1016/j.neurad.2009.03.001

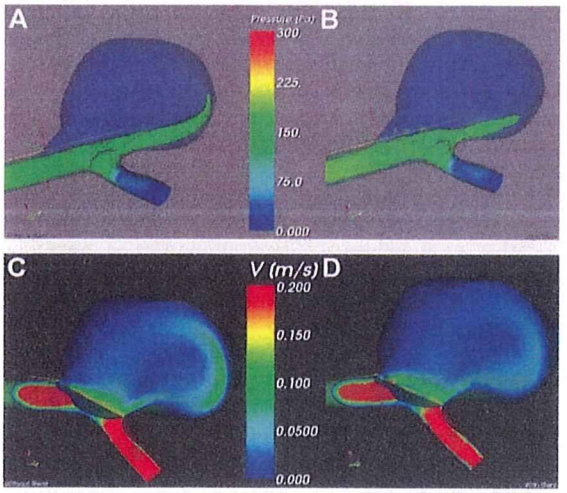

Figure 3 Isovelocity surface (0.1 m/s) colored in pressure without device (A) and with device (B), velocity magnitude in cross-sectional and neck planes, without device (C), and with device (D).

and temporal developed velocity profiles (Womersley profiles). A virtual stent was further inserted in the parent artery and flow was computed. The efficiency of the stent to reduce flow and vorticity within the aneurysm was assessed. Although a residual flow remains inside the aneurysm, a reduction of the jet entering the aneurismal cavity can be observed (Fig. 3B). It can be noticed that the Z-like stent, presenting in this case an open-cell design and a rather large porosity of 82%, is still able to reduce somewhat the entry of flow from the parent artery. This reduction is small because stent porosity is high (82%). Stents currently under development aim at much lower porosities so as to increase much greater flow entry impediment.

In order to demonstrate the clinical value of numerical simulations of the effects of stent on intra-aneurismal flow, the Virtual Intracranial Stenting Challenge (VISC'07, [44][1]) was launched and discussed at the 4th Intracranial Stent Meeting (ICS'07, Kyoto). Its objectives were to compare state-of-the-art numerical approaches for solving flow in a stented human cerebral aneurysm model and to illustrate the ability of academic groups and leading CFD companies in providing a description of changes in aneurismal blood flow patterns for a given stent design. The adopted methodology, as well as simulation parameters, software and hardware choices, simulation times, stent performances were compared. Although some differences in the magnitude of the computed WSS and the velocity field were reported, it was demonstrated that numerical simulations were reproducible among teams. The VISC'07 reinforced the potential role of CFD simulations in providing a description of patient-specific blood flow information in clinical settings, enabling the virtual evaluation of stent performances. The ultimate goal is to use such methods for the selection of an appropriate stent prior to intervention. Also, the same methodology can be used by stent manufacturers for performance analysis and development of novel stent designs.

Discussion/conclusion

Flow is believed to be a major actor in the initiation, growth and rupture of cerebral aneurysms, hence, the interest for the development of methodologies allowing for the assessment of blood flow within the aneurysm and the flow-driven biomechanical effects.

The modeling of such complex systems must be further improved by including wall motion, wall stress, mechanotransduction at the endothelial and medial cell level and clot formation mechanics.

Due to the complex modeling of patient-specific aneurysm geometries and endovascular prosthesis representations, experimental setups allowed for the understanding of aneurismal hemodynamical effects due to a stent or a coil prior to numerical approaches.

The most common methodologies to assess blood flow in cerebral aneurysm models are PIV and numerical simulations. Patient specific numerical simulations approaches have the potential to become the method of choice for planning, treatment and follow-up decisions. Numerical simulations have proved to be reproducible among teams and to be quite similar to experimental observations and measurements and may therefore become a post-processing path-empowering personalized treatment strategies. However, in order to increase their impact and general acceptance, further efforts are needed to reach agreement between experimental and virtual worlds. Should numerical analysis of blood flow in aneurysms reach the level of being precise and fast enough to be seamlessly integrated with the imaging procedures, physicians would possess a valuable tool for assessing the effects of flow and the impact of their gestures on local hemodynamics in a quantitative way. We may imagine that numerical simulations could be carried out at the moment a patient enters in a hospital and integrated in the medical image acquisition modalities. Results would arrive in time allowing treating physicians to decide on treatment modality. A personalized treatment could be subsequently proposed.

This objective in mind, a sixth framework programme (information society technology, FP6-IST), @neurIST [2] is aiming at developing the required IT for supporting a management that can integrate the complexity of data made available with modern medicine of cerebral aneurysms.

Conflict of interests

No potential conflict of interests relevant to this article was reported.

Acknowledgments

Enabled by the Swiss National Research Foundation (Grant Number 3252B0-105735/1) and receiving additional support from the Egon Naef Foundation for in vitro research (Geneva, Switzerland, www.fondation-naef.com), this work was generated in the framework of the @neurIST Project, which is

[1] http://www.cilab.upf.edu/visc06/.

[2] www.aneurist.org.

Please cite this article in press as: Augsburger L, et al. Methodologies to assess blood flow in cerebral aneurysms: Current state of research and perspectives. J Neuroradiol (2009), doi:10.1016/j.neurad.2009.03.001

co-financed by the European Commission through the contract no. IST-027703.

We would like to express our best thanks to Mr Louis Auer (www.elastrat.com, Geneva, Switzerland) for developing and providing the silicone vascular models.

The authors also wish to warmly thank Dr Tiziano Binzoni, PhD, Dr Alessandro G. Radaelli, PhD for their precious advices, Dr Fumio Asakura, MD, and all the technicians from the Hydraulic Machines Laboratory (lmh.epfl.ch, Lausanne, Switzerland) for their support and help in conducting the measurements.

References

[1] Humphrey JD (2002). Cardiovascular solid mechanics: cells, tissues, and organs. Springer-Verlag, New-York, 757 pp.
[2] Weir BK, et al. Cigarette smoking as a cause of aneurysmal subarachnoid hemorrhage and risk for vasospasm: a report of the Cooperative Aneurysm Study. J Neurosurg 1998;89: 405–11.
[3] Cloft HJ, et al. Prevalence of cerebral aneurysms in patients with fibromuscular dysplasia: a reassessment. J Neurosurg 1998;88:436–40.
[4] Schievink WI, et al. Intracranial aneurysm surgery in Ehlers-Danlos syndrome Type IV. Neurosurgery 2002;51:607–11 [discussion 611–3].
[5] Cannon Albright LA, et al. A genealogical assessment of heritable predisposition to aneurysms. J Neurosurg 2003;99: 637–43.
[6] Vernooij MW, et al. Incidental findings on brain MRI in the general population. N Engl J Med 2007;357:1821–8.
[7] Wiebers DO, et al. Unruptured intracranial aneurysms: natural history, clinical outcome, and risks of surgical and endovascular treatment. Lancet 2003;362:103–10.
[8] San Millan Ruiz D, et al. The perianeurysmal environment: influence on saccular aneurysm shape and rupture. AJNR Am J Neuroradiol 2006;27:504–12.
[9] Frosen J, et al. Remodeling of saccular cerebral artery aneurysm wall is associated with rupture: histological analysis of 24 unruptured and 42 ruptured cases. Stroke 2004;35: 2287–93.
[10] Kim LJ, Klopfenstein JD, Spetzler RF. Clip reconstruction and sling wrapping of a fusiform aneurysm: technical note. Neurosurgery 2007;61(Suppl. 3):79–80 [discussion 80].
[11] Molyneux AJ, et al. International subarachnoid aneurysm trial (ISAT) of neurosurgical clipping versus endovascular coiling in 2143 patients with ruptured intracranial aneurysms: a randomised comparison of effects on survival, dependency, seizures, rebleeding, subgroups, and aneurysm occlusion. Lancet 2005;366:809–17.
[12] van der Schaaf I, et al. Endovascular coiling versus neurosurgical clipping for patients with aneurysmal subarachnoid haemorrhage. Cochrane Database Syst Rev 2005;4:CD003085.
[13] Rufenacht D, et al. Current concepts of endovascular aneurysm treatment, and about the role of stents for endovascular repair of cerebral arteries. Schweiz Arch Neurol Psychiatr 2004;155:348–52.
[14] Cebral JR, et al. Efficient pipeline for image-based patient-specific analysis of cerebral aneurysm hemodynamics: technique and sensitivity. IEEE Trans Med Imaging 2005;24:457–67.
[15] Kim C, et al. In vivo study of flow pattern at human carotid bifurcation with regard to aneurysm development. Acta Neurochir (Wien) 1992;115:112–7.
[16] Nakatani H, et al. In vivo flow visualization of induced saccular cerebral aneurysms in rats. Acta Neurochir (Wien) 1993;122:244–9.
[17] Chong BW, et al. Blood flow dynamics in the vertebrobasilar system: correlation of a transparent elastic model and MR angiography. AJNR Am J Neuroradiol 1994;15:733–45.
[18] Lieber BB, Stancampiano AP, Wakhloo AK. Alteration of hemodynamics in aneurysm models by stenting: influence of stent porosity. Ann Biomed Eng 1997;25:460–9.
[19] Rhee K, Han MH, Cha SH. Changes of flow characteristics by stenting in aneurysm models: influence of aneurysm geometry and stent porosity. Ann Biomed Eng 2002;30:894–904.
[20] Barath K, et al. Influence of stent properties on the alteration of cerebral intra-aneurysmal haemodynamics: flow quantification in elastic sidewall aneurysm models. Neurol Res 2005;27(Suppl. 1):S120–8.
[21] Barath K, et al. Anatomically shaped internal carotid artery aneurysm in vitro model for flow analysis to evaluate stent effect. AJNR Am J Neuroradiol 2004;25:1750–9.
[22] Lieber BB, et al. Particle image velocimetry assessment of stent design influence on intra-aneurysmal flow. Ann Biomed Eng 2002;30:768–77.
[23] Canton G, et al. Flow changes caused by the sequential placement of stents across the neck of sidewall cerebral aneurysms. J Neurosurg 2005;103:891–902.
[24] Yu SC, Zhao JB. A steady flow analysis on the stented and non-stented sidewall aneurysm models. Med Eng Phys 1999;21: 133–41.
[25] Liou TM, Chang WC, Liao CC. LDV measurements in lateral model aneurysms of various sizes. Exp Fluid 1997;23:317–24.
[26] Tateshima S, et al. In vitro measurement of fluid-induced wall shear stress in unruptured cerebral aneurysms harboring blebs. Stroke 2003;34:187–92.
[27] Hollnagel DI, et al. Laser Doppler velocimetry (LDV) and 3D phase-contrast magnetic resonance angiography (PC-MRA) velocity measurements: validation in an anatomically accurate cerebral artery aneurysm model with steady flow. J Magn Reson Imaging 2007;26:1493–505.
[28] Steinman DA, et al. Image-based computational simulation of flow dynamics in a giant intracranial aneurysm. AJNR Am J Neuroradiol 2003;24:559–66.
[29] Cebral JR, Hernandez M, Frangi AF. Computational analysis of blood flow dynamics in cerebral aneurysms from CTA and 3D rotational angiography image data. In: Doblaré AF, Cerrolaza M, Rodrigues H, editors. International congress on computational bioengineering. 2003.
[30] Cebral JR, et al. Characterization of cerebral aneurysms for assessing risk of rupture by using patient-specific computational hemodynamics models. AJNR Am J Neuroradiol 2005;26:2550–9.
[31] Ortega HV. Computer simulation helps predict cerebral aneurysms. J Med Eng Technol 1998;22:179–81.
[32] Cebral JR, et al. Blood-flow models of the circle of Willis from magnetic resonance data. J Eng Math 2003;47:369–86.
[33] Valencia A, et al. Blood flow dynamics in patient-specific cerebral aneurysm models: The relationship between wall shear stress and aneurysm area index. Med Eng Phys 2008;30(3):329–40. Epub 2007.
[34] Hassan T, et al. Computational replicas: anatomic reconstructions of cerebral vessels as volume numerical grids at three-dimensional angiography. AJNR Am J Neuroradiol 2004;25:1356–65.
[35] Ohta M, et al. Rheological changes after stenting of a cerebral aneurysm: a finite element modeling approach. Cardiovasc Intervent Radiol 2005;28:768–72.
[36] Aenis M, Stancampano AP, Wakhloo AK, Lieber BB. Modeling of flow in a straight stented and nonstented side wall aneurysm model. J Biomech Eng 1997;119(2):206–12.
[37] Stuhne GR, Steinman DA. Finite-element modeling of the hemodynamics of stented aneurysms. J Biomech Eng 2004;126: 382–7.

Please cite this article in press as: Augsburger L, et al. Methodologies to assess blood flow in cerebral aneurysms: Current state of research and perspectives. J Neuroradiol (2009), doi:10.1016/j.neurad.2009.03.001

[38] Cebral JR, Lohner R. Efficient simulation of blood flow past complex endovascular devices using an adaptive embedding technique. IEEE Trans Med Imaging 2005;24:468–76.
[39] Appanaboyina S, et al. Computational fluid dynamics of stented intracranial aneurysms using adaptive embedded unstructured grids. Int J Numerical Methods Fluids 2008;57: 475–93.
[40] Hirabayashi M, et al. Characterization of flow reduction properties in an aneurysm due to a stent. Phys Rev E Stat Nonlin Soft Matter Phys 2003;68:021918.
[41] Chopard B, et al. Lattice Boltzmann modeling of thrombosis in giant aneurysms. Int J Mod Phys C 2007;18:712–21.
[42] Chopard B, Ouared R, Rufenacht D. A lattice Boltzmann simulation of clotting in stented aneursysms and comparison with velocity or shear rate reductions. Math Comput Sim 2006;72: 108–12.
[43] Tateshima S, et al. Intraaneurysmal flow visualization by using phase-contrast magnetic resonance imaging: feasibility study based on a geometrically realistic in vitro aneurysm model. J Neurosurg 2004;100:1041–8.
[44] Radaelli AG, et al. Reproducibility of haemodynamical simulations in a subject-specific stented aneurysm model – A report on the Virtual Intracranial Stenting Challenge 2007. J Biomech 2008;41(10):2069–81. Epub 2008.

Please cite this article in press as: Augsburger L, et al. Methodologies to assess blood flow in cerebral aneurysms: Current state of research and perspectives. J Neuroradiol (2009), doi:10.1016/j.neurad.2009.03.001

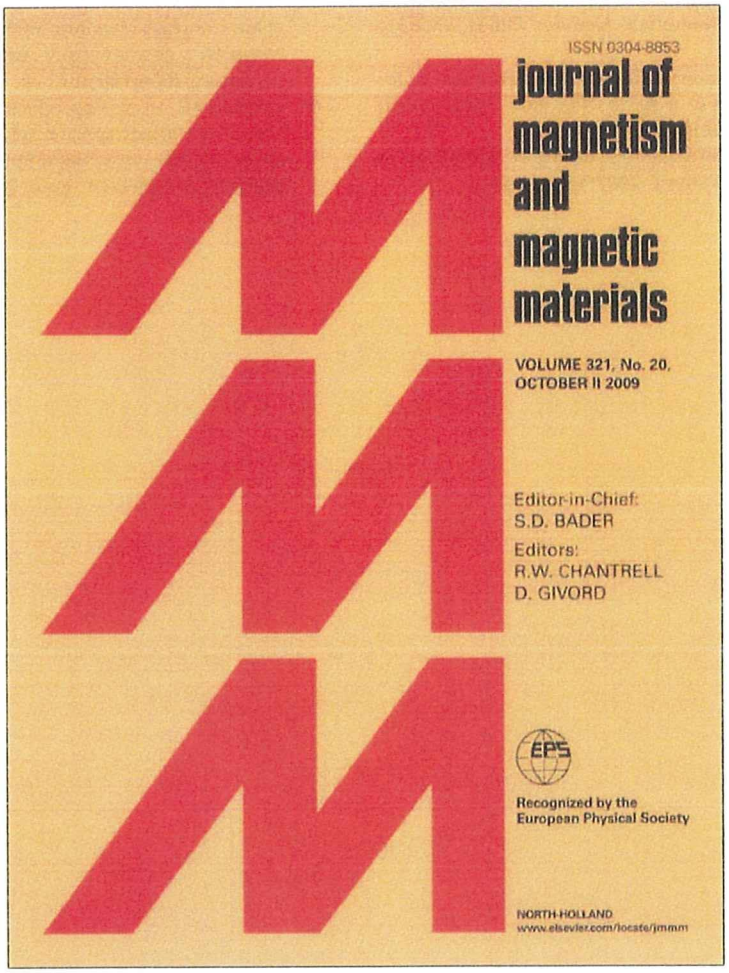

Journal of Magnetism and Magnetic Materials 321 (2009) 3483–3487

Contents lists available at ScienceDirect

Journal of Magnetism and Magnetic Materials

journal homepage: www.elsevier.com/locate/jmmm

Heat diffusion characteristics of magnetite nanoparticles dispersed hydro-gel in alternating magnetic field

Makoto Suto [a], Hiroyuki Kosukegawa [b], Kaoru Maruta [b], Makoto Ohta [b], Kazuyuki Tohji [a], Balachandran Jeyadevan [a,*]

[a] Graduate School of Environmental Studies, Tohoku University, Sendai, Japan
[b] Institute of Fluid Science, Tohoku University, Sendai, Japan

ARTICLE INFO

Article history:
Received 15 January 2009
Received in revised form
11 June 2009
Available online 27 June 2009

Keywords:
Hyperthermia
Heat diffusion
Magnetite
Magnetic fluid
AC magnetic field

ABSTRACT

Heat diffusion characteristics of a spherical heat source dispersing magnetite nanoparticles (MNPs) in hydro-gel were investigated numerically and experimentally to evaluate the conditions required for magnetic fluid hyperthermia (MFH). Numerical estimation assumed one-dimensional spherical model and constant heat evolution. Experimental observation was carried out by exposing the magnetite-dispersed hydro-gel in an AC magnetic field with strength and frequency of 3.2 kA/m and 600 kHz, respectively. The temperature distribution observed along the radial axis of the spherical heat source agreed well with the theoretical estimation quantitatively and qualitatively. However, the minor difference existed between the theory and experiment was due to the variation in experimentally determined and actual particle size distributions. Thus, we could conclude that the proposed algorithm could be extended to be used in the estimation of the temperature distribution in intravital conditions with blood flow, metabolism etc., to arrive at biologically significant conclusions helpful for MFH cancer treatment.

1. Introduction

Cancer is treated by using surgery, radiotherapy, chemotherapy and immune therapy and each of them has their own merits and demerits. Apart from the conventional methods, magnetic fluid hyperthermia (MFH), which necroses the cancer tissues by the heat generated from the magnetic particles exposed to alternating magnetic field, has been proposed to be used either alone or in conjunction with the already existing conventional therapy for enhanced treatment. The main advantage of magnetic hyperthermia technique is that it could raise the temperature of cancer tissue selectively. Recent reports have claimed the effectiveness of MFH in treating prostate cancer and glioblastoma [1–3]. However, details pertaining to some basic information, such as (a) the optimum particle diameter, (b) magnetic nanoparticles (MNPs) concentration necessary to elevate the temperature of the target volume above 43 °C and also (c) the temperature distribution inside and outside the target region, are limited. The above information is vital to provide required level of therapeutic temperature with minimum magnetic particle concentration and also to avoid damaging of the surrounding normal tissue through overheating.

Andrä et al. [4] numerically estimated the heat diffusion characteristics of constant power density spherical heat source surrounded by a homogeneous heat conductive media and also experimentally verified the same by dispersing micron-sized particle in the cylindrical muscle tissue of cow. They reported a reasonable agreement between numerical estimation and experimental observation [4]. However, it should be noted that the heating mechanism in the above study was different to the one in MFH. On the other hand, Hergt et al. [5] numerically estimated the temperature distribution in a spherical heat source dispersing MNP. And also, they investigated non-spherical and spherical-shaped organic gel models experimentally. However, their experimental study was limited to measuring the temperature at the surface of the heat source. Recently, Wang et al. [6] assessed the heating effect *in-vivo* by preparing magnetite suspension dispersing particles with various average diameters. Though they found that MNP can generate enough power for effective MFH, information on the physical properties of the particles such as size distribution, blocking temperature, etc. were not reported. Furthermore, studies related to materials suitable for MFH has been carried out and magnetite has been considered most suitable from the stand point of magnetic property and biocompatibility.

Thus in this study, we have investigated the concentration dependence of MNP on heat diffusion characteristics. We report the one-dimensional numerical calculation and experimental results of heat diffusion characteristics of spherical heat source

* Corresponding author. Tel./fax: +81 22 795 7412.
E-mail address: jeya@mail.kankyo.tohoku.ac.jp (B. Jeyadevan).

0304-8853/$ - see front matter © 2009 Elsevier B.V. All rights reserved.
doi:10.1016/j.jmmm.2009.06.067

(diameter: 25 mm) dispersing MNPs of various weight fractions (average particle diameter: 13.5 nm) in hydro-gel surrounded by magnetite-free hydro-gel simulating cancer and normal tissues, respectively.

2. Numerical investigation

Heat dissipation of MNPs used in this experiment is caused by the delay in the relaxation of their magnetic moments in an AC magnetic field and is given by the following equation [7]:

$$P = \mu_0 \chi'' f H_{apply}^2 \tag{1}$$

where μ_0 is the permeability of free space, χ'' the magnetic susceptibility (imaginary part), f the frequency of applied AC magnetic field and $H_{applied}$ the strength of applied AC magnetic field. The TEM micrograph and size distribution of MNP are shown in Figs. 1 and 2. The particle distribution is fitted with the Gaussian distribution. The magnitude of heat dissipated from heat source dispersing 1, 2 and 4 wt% of MNPs are estimated using Eq. (1) and particle size distribution shown in Fig. 2. Their values are 84.4, 170.4 and 346.6 kJ/m^3, respectively.

A numerical model is constructed to calculate the one-dimensional heat diffusion characteristics of the heat source dispersing MNPs in hydro-gel are shown in Fig. 3(a). The heat source (radius of $a = 12.5$ mm) in an alternating magnetic field is assumed to dissipate constant power. And also, the magnetite-dispersed spherical heat source is assumed to be surrounded by particle free hydro-gel ($a<r<b$). Additionally, we have assumed the above spherical composite (magnetite-dispersed hydro-gel and magnetite-free hydro-gel) sphere is surrounded by a layer of air ($b<r<R$). The radius of b and effective radius, R are calculated by the following equation:

$$r = 3 \times \frac{Volume}{Surface\ area} \tag{2}$$

The radius of b and R are 21.1 and 31.0 mm, respectively.

The governing equations for the one-dimensional heat diffusion are as follows:

$$\rho c \frac{\partial T_1}{\partial t} = \frac{1}{r^2}\frac{\partial}{\partial r}\left(kr^2 \frac{\partial T_1}{\partial t}\right) + Q(0<r<a) \tag{3a}$$

$$\rho c \frac{\partial T_2}{\partial t} = \frac{1}{r^2}\frac{\partial}{\partial r}\left(kr^2 \frac{\partial T_2}{\partial t}\right)(a<r<b) \tag{3b}$$

$$\rho c \frac{\partial T_3}{\partial t} = \frac{1}{r^2}\frac{\partial}{\partial r}\left(kr^2 \frac{\partial T_3}{\partial t}\right)(b<r<R) \tag{3c}$$

where ρ is the density of mass, c the specific heat, k the heat conductivity, r the distance from the center of heat source (sphere dispersing MNP), T the temperature (T_1 is the temperature in the heat source, T_2 the temperature in the surrounding media and T_3 is the temperature in the layer of air) and Q the heat evolution.

The initial and boundary conditions are

$$T_1(r,0) = T_2(r,0) = T_3(r,0) = T_e \tag{4}$$

$$\left(\frac{\partial T_1}{\partial r}\right) = 0 \tag{5}$$

$$\left(\frac{\partial T_1}{\partial r}\right) = \left(\frac{\partial T_2}{\partial r}\right)(r = a) \tag{6}$$

$$\left(\frac{\partial T_2}{\partial r}\right) = \left(\frac{\partial T_3}{\partial r}\right)(r = b) \tag{7}$$

where T_e is the initial temperature (290.15 K). The ρ, c and k of magnetite-dispersed hydro-gel are measured by using Archimedes, differential scanning calorimetry (DSC) and unsteady hot wire methods, respectively. The results are shown in Table 1. Calculation was performed by digitizing Eqs. (3a)–(3c) by using the complete implicit method and solved by tri-diagonal matrix algorithm.

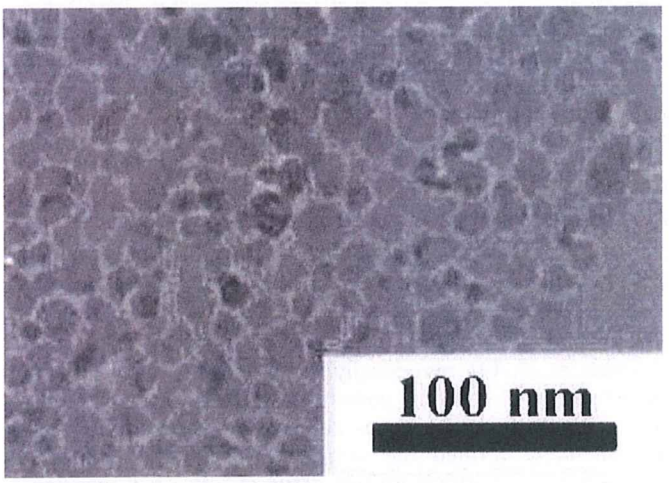

Fig. 1. Transmission electron micrograph of magnetite nanoparticles.

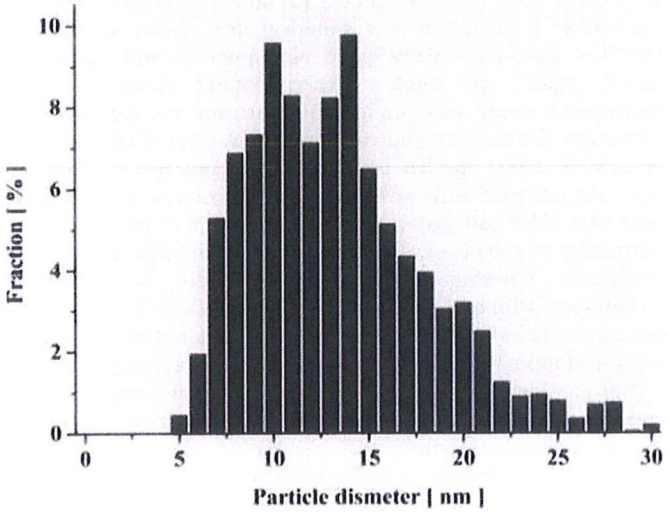

Fig. 2. Size distributions of magnetite nanoparticles.

3. Experimental investigation

The magnetite particles used in this study are water-dispersed magnetic fluid supplied by Taiho Kougyo Ltd., Japan. The first surfactant layer around the magnetite nanoparticle surface is oleate and with this alone the particles cannot be dispersed in water. The details of the surfactant used as second layer is not disclosed by the supplier. But it should be noted that the dispersion of the particles in water itself indirectly implies that the particles are coated with a second layer.

In accordance with the numerical model, 25 mm diameter spherical heat source dispersing MNPs in hydro-gel was prepared. The magnetite particles suitable for hyperthermia should dissipate heat through Neel relaxation, which does not depend on the viscosity of the local environment. Thus, the particles were dispersed in hydro-gel, which inhibits the rotation of the

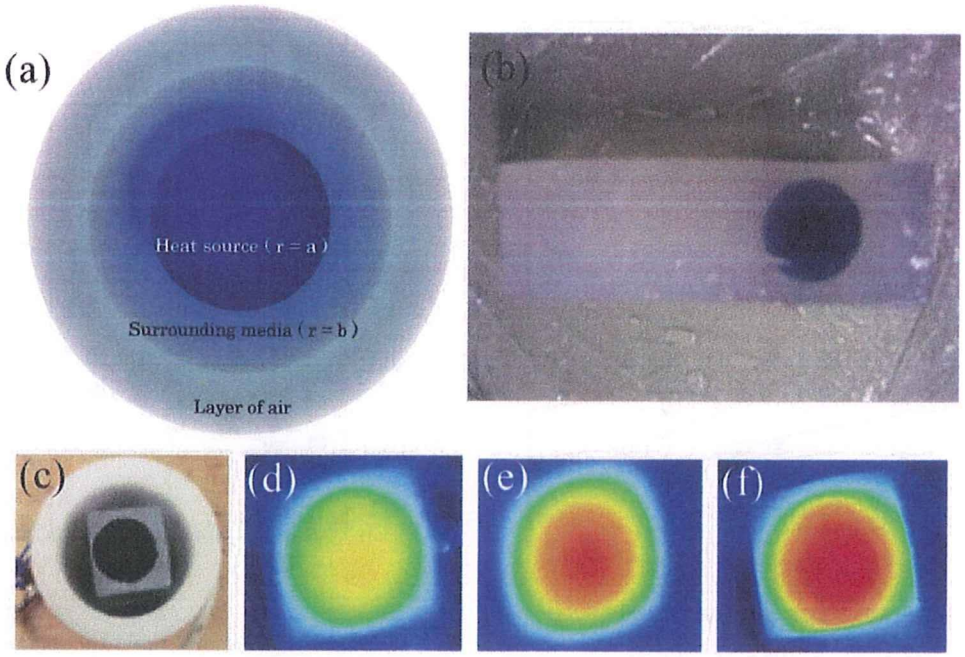

Fig. 3. Schematic diagram of (a) numerical model (the length of a, b and R are 12.5 mm, 20.11 mm and 1 m, respectively) and photographs of (b) experimental specimen (spherical heat source dispersing magnetite in hydro-gel, covered with magnetite-free hydro-gel), (c) cross-section of heat source placed inside the coil and (d)–(e) thermal views of the specimen exposed to varying AC magnetic field exposure time.

Table 1
Physical properties of hydro-gel and hydro-gel dispersing various concentrations (1, 2, 4 wt%) of MNPs.

Materials	k ($W m^{-1} K^{-1}$)	Cp ($J kg^{-1} K^{-1}$)	P ($g cm^{-3}$)
Hydro-gel	0.2536	2.759	1
1 wt%	0.2882	2.995	1.001
2 wt%	0.3043	3.197	1.009
4 wt%	0.3683	2.786	1.026

magnetite particles exposed to AC magnetic field and simulates that worst situation that may prevails *in-vivo*. The procedure used for the preparation of hydro-gel is as follows: first, 6:4 mixture of dimethylsulfoxide (DMSO) and water were prepared. Then, 10 wt% of PVA was added to the mixture and mixed vigorously for 2 h (at 90 °C) to obtain the sol. Finally, the sol was poured into a spherical mold and cooled in a deep freezer. The experimental specimen was prepared by surrounding the magnetite-dispersed hydro-gel with magnetite-free rectangular hydro-gel block. The photograph of the (b) experimental specimen, (c) cross-section of heat source (hydro-gel dispersing magnetite) surrounded by magnetite-free hydro-gel placed inside the coil and the thermal view of the specimen exposed to varying AC magnetic field exposure time (d)–(f) are shown in Fig. 3. Heat source dispersing 1, 2, 4 wt% of magnetite were prepared to study the influence of MNP concentration on heating capacity and temperature distribution.

The heat diffusion characteristics of the MNP was determined by placing the specimen inside the coil and exposing the same to AC magnetic field strength and frequency of 3.2 kA/m and 600 kHz, respectively. Temperature at various points inside the heat source was measured by using a 3 mm diameter alcohol thermometer. The positions of measuring points were determined using X-ray photography. Since the coefficient of thermal conductivity of silica glass is higher than PVA-gel, the glass is heated better than the hydro-gel and also could conduct the heat well. Consequently, the heat can escape through the thermometer and some degree of influence is anticipated. However, the specific heat of hydro-gel is about three times that of silica glass and the influence towards heat conduction is considered comparatively small.

4. Results and discussion

Numerically calculated and experimentally observed temperature distributions for 1, 2 and 4 wt% of magnetite are shown in Fig. 4. The calculated as well as experimentally observed temperature rise at the center of the heat source is larger than that at the surface, and the temperature gradient at the surface was steep. Though the temperature of the human body is 36–37 °C, we set the initial temperature at 17 °C to compare the numerical and experimental values. Since the cancer tissue is claimed to become necrotic at 43°, the temperature should be raised only by 6–7 °C. Hence, the results indicate that 2 wt% magnetite is sufficient for therapy, if metabolism and blood perfusion are ignored. Additionally, the temperature at a distance of 15 mm from the center of the heat source was much lower than that at the surface. This confirmed the local heating characteristics of MFH.

Though quantitative and qualitative agreement between numerical calculation and experimental observations was recorded, minor quantitative deviation was observed for all three solid concentrations considered in this study. The deviation became larger with increasing particle concentration. In the above study, the numerical calculation and experiments were carried fixing the AC magnetic field exposure time to 600 s, due to the operational limitations posed by the instrument. Thus, the deviation could also be considered due to the difference in temperature increment rate between numerical calculation and experimental observation. Thus, the validity of this behavior under steady state was examined by carrying out simulation as well as experiments for longer periods of time. The results confirmed that the deviation was not due to the difference in temperature increment rate. Another possible factor that could have contributed to the variation is the heat generated from the coil. This was also confirmed negative.

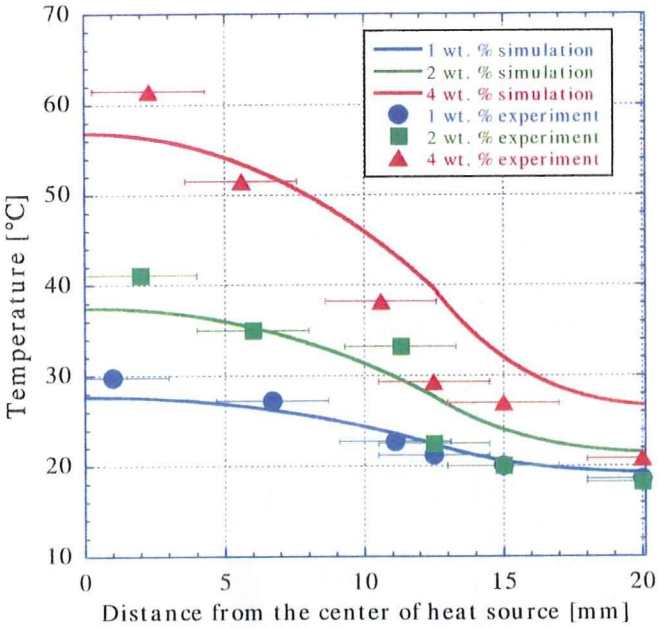

Fig. 4. Comparison between numerically estimated and experimentally observed temperature distributions.

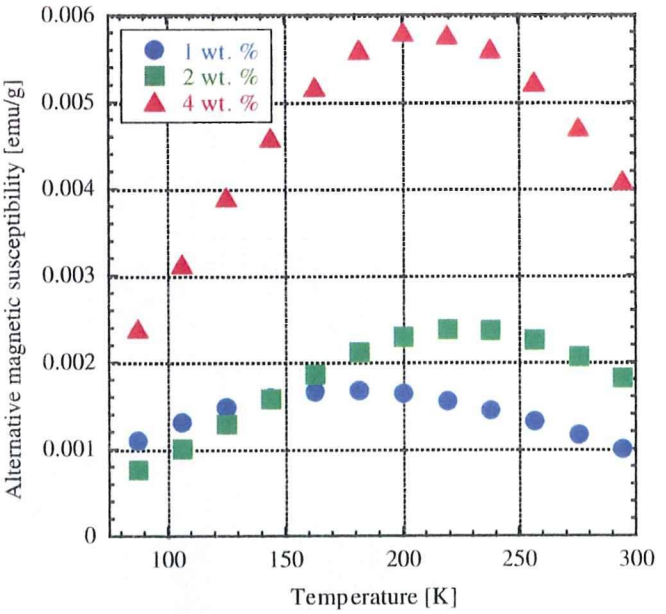

Fig. 5. The imaginary part of magnetic susceptibility as a function of temperature for the hydro-gel dispersing various concentrations of magnetite (frequency: 9 kHz).

The other possible reasons could be due to either the magnetic interaction among particles caused by the decrease in the inter particle distance associated with the increase in particle concentration or the difference between the actual and estimated particle size distribution from the TEM pictures. In the former case, the minimum inter particle distance is determined by the surfactant layer thickness. However, it should be noted that the MNP used in this study are coated with two layers of surfactants. It has been reported that the distance maintained by the surfactant layer is far enough to prevent the magnetic interaction between particles [8]. Furthermore, the AC magnetic susceptibility was measured to investigate the magnetic characteristics of the hydro-gel with different magnetite concentration. The imaginary part of magnetic susceptibility as a function of temperature for the hydro-gel dispersing various concentrations of magnetite is shown in Fig. 5. The temperature at which the χ'' is maximum (χ'' max) for a measuring frequency of 10 kHz for 2 and 4 wt% MNP shifted to higher temperature compared to 1 wt%. If the shift in χ'' max between 1 and 2 wt% MNP is assumed as a consequence of magnetic interaction, then the 4 wt% MNP is expected to have higher magnetic interaction and χ'' max should shift to much higher temperature. However, the experimentally observed peak positions do not show any considerable shift meaning that the difference in peak position observed between 1 and 2 wt% MNP was due to the variation in the actual and estimated particle size distribution. The shift in the χ'' max is within the limits of the particle size variation found from our TEM observation. Thus, we conclude that the disparity in temperature distribution between the numerical calculation and experimental observation was due to the difference between the actual particles size distribution and the one estimated from the TEM measurements.

In MFH treatment, minimum use of MNP concentration is desirable. This could be achieved by using MNP with optimum diameter with narrow size distribution. Though the optimum particle diameter is yet to be verified experimentally, the average blocking temperature of magnetite sample that could generate considerable heat has been proposed [9]. Considering the fact that the temperature necessary to be maintained within the cancer tissue should be higher than 43 °C, and blood perfusion that removes part of the heat generated away, at least 2 wt% of magnetite is necessary to raise the temperature in a 12.5 mm diameter sphere. However, it should be noted that the physical properties of hydro-gel such as specific heat, heat conductivity, mass density, etc. are different from the human cells. The above numerical and experimental studies on MFH have suggested that the existing theories proposed for heat generation and dissipation could be used to extend this model to analyze the temperature distribution considering blood flow in cancer tissues. Thus, the final goal of this study is to numerically model the temperature distribution in a cancer tissue taking the blood flow and metabolism into consideration.

5. Conclusions

In this study, we have investigated the heat diffusion characteristics of MNPs dispersed in hydro-gel numerically and experimentally. Although quantitative and qualitative agreement between experimental observation and numerical calculations for a heat source dispersing MNP with various solid concentrations were observed, minor quantitative deviations were observed due to the differences in the estimated and actual particle-sized distribution. The appropriate concentration of magnetite necessary to maintain the required temperature elevation was 2 wt% or above. However, considering the magnetic properties of the sample it was proposed that similar temperature rise could be practically achieved using even 1 wt% of magnetite with enhanced magnetic property. It should be noted that the blood flow and the heat transport due to flow should be considered when the heat conduction within the body is studied. The results have suggested that the present model could be extended to incorporate intravital factors such as blood flow, metabolism etc. to arrive at biologically significant conclusions.

Acknowledgment

This work was supported by Grant-in-Aid for Basic Research #(A) 17201021 from the Ministry of Education, Science, Culture and Sport of Japan. We thank Dr. Fujita from Graduate School of

Journal of Biomechanical Science and Engineering

Vol. 5, No. 1, 2010

Development of an In Vitro Tracking System with Poly (vinyl alcohol) Hydrogel for Catheter Motion*

ChangHo YU[**], Hiroyuki KOSUKEGAWA[***], Keisuke MAMADA[**], Kanju KUROKI[****], Kazuto TAKASHIMA[*****], Kiyoshi YOSHINAKA[******] and Makoto OHTA[****,†]

** Graduate School of Biomedical Engineering, Tohoku University,
2-1-1 Katahira, Aoba-ku, Sendai, Miyagi 980-8577, Japan
E-mail: changho_yu@biofluid.ifs.tohoku.ac.jp
*** Graduate School of Engineering, Tohoku University,
6-6 Aoba, Aramaki, Aoba-ku, Sendai, Miyagi 980-8579, Japan
**** Institute of Fluid Science, Tohoku University,
2-1-1 Katahira Aoba-ku, Sendai, Miyagi 980-8577, Japan
***** RIKEN-TRI Collaboration Center for Human-Interactive Robot Research, RIKEN,
2271-130, Anagahora, Shimoshidami, Moriyama-ku, Nagoya, Aichi 463-0003, Japan
****** Department of Bioengineering, The University of Tokyo,
7-3-1, Hongo, Bunkyo-ku, Tokyo 1138656, Japan

Abstract

Vascular diseases, such as ischemic heart disease, infarction, aneurysms, stroke and stenosis are a leading cause of serious long-term disability and their mortality rate is as high as that of cancers in many countries. Recently, neurovascular intervention using catheters is a minimally-invasive endovascular technique used to treat vascular disease of the brain, and a navigation system for catheters has been developed to facilitate surgical planning and to provide intra-operative assistance. Since the mechanical properties of a catheter play an important role in reaching the targeted disease, tracking of catheter movement during endovascular treatment may be useful to increase confirmation of the rate of successful operation. In this study, we developed an in vitro tracking system for catheter motion using poly (vinyl alcohol) hydrogel (PVA-H) to mimic an arterial wall. The employed models were made of PVA-H, which is sufficiently transparent to permit observation of catheter movement in the artery. This system is expected to contribute to validation of computer-based navigation systems for surgical assistance.

Key words: Endovascular Treatment, Catheter Motion, Tracking System, Poly (vinyl alcohol) Hydrogel, Biomodel

1. Introduction

Vascular diseases are a leading cause of serious long-term disability and their mortality rate is as high as that of cancer in many countries [(1)]. Moreover, cerebrovascular disease ranks third both in the United States and in Japan annually as a cause of death, resulting in more than 160,000 and 127,000 deaths respectively[(2), (3)]. Catheters are used for transporting drugs and implants, as well as for observation, diagnosis or treatment of infarction, aneurysms and stenosis in the endovasculature. Recently, endovascular treatment using catheters has been proven to be useful as a less invasive treatment modality [(4)-(6)], and thus, the number of the cases so treated has increased.

To reach and treat a diseased part with a catheter, physicians manipulate and control the

*Received 3 June, 2009 (No. 09-0243)
[DOI: 10.1299/jbse.5.11]

catheter by means of angiographic monitors. The techniques of such treatment have gradually been improved and a catheter simulator for navigation has been developed [7], [8]. Takashima et al. developed a computer-based navigation system for operation assistance [9], [10]. Since the navigation system they developed is based on applied force and balance, reconstruction of the geometry and force field may be important. To validate such a computer-based navigation system, tracking the motion of a catheter is necessary and an in vitro transparent model with mechanical properties and geometries similar to those of a real artery, termed a biomodel, may be useful.

Ohta et al. developed a biomodel using poly (vinyl alcohol) hydrogel (PVA-H), as shown in Fig. 1(a) [11]. The mechanical properties, such as Young's modulus, of PVA-H are controllable with various techniques. For example, Kosukegawa et al. have described ways to elucidate the mechanical properties of biomodels using various concentrations of PVA solution, degrees of polymerization, saponification values and blending techniques [12]. Mamada et al. have reported that sensory evaluation of such procedures as touching, suturing or cutting of the PVA-H mucosa model, shown in Fig. 1(b), yields higher scores than those of a conventional material [13]. These results suggest that the force and balance field of an artery wall can be reconstructed by a PVA-H biomodel.

In the present study, utilizing a PVA-H model, we examined catheter movement for development of an in vitro tracking system and evaluated the system by observation of video recordings of catheter motion.

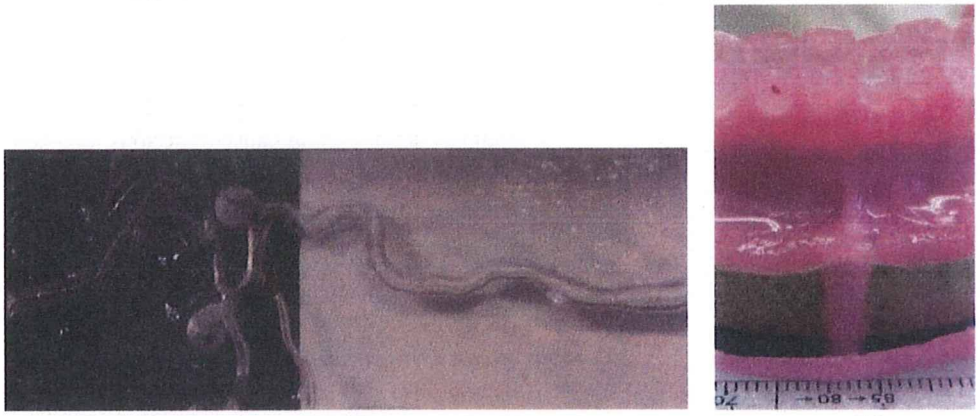

(a) (b)

Fig. 1 Examples of PVA-H biomodels : (a) PVA-H biomodel of endovasculature (b) Biomodel of oral muscosa using PVA-H

2. Experimental Methods

2.1 Gelation of PVA and Lost wax Technique

PVA (JAPAN VAM & POVAL CO., LTD., Japan) was dissolved in a mixed solvent of dimethyl sulfoxide (DMSO) (Toray Fine Chemicals Co., Ltd., Japan) and distilled water (80/20, w/w) [12]. The PVA powder in the mixture solution was stirred for 2 hours at 100°C until dissolution. This PVA solution was then cast into an acrylic box with a mold to make a PVA-H box model having realistic geometry and cross geometry, as shown by Figs. 2(a) and (c) and described in the following section. The two different PVA-H models shown in Figs. 2(b) and (d) were used for catheter tracking and motion capture. These models were maintained at -30°C for 24 hours to promote PVA crystallization. After gelation, the mold material was removed using water as in the lost-wax technique [14].

2.2. Cross geometry of the PVA-H model for Tracking System and Motion Capture of Catheter

A mold with crossing branches, shown as Fig. 3(a), was constructed using Magics software (Magics RP 8.5; Materialise, Leuven, Belgium). The diameter of the main artery was set at 4 mm as a mean of the intracranial artery [15], [16]. A zebra pattern (2 mm long and 2 mm thick) was painted on a catheter [2.9/2.4 Fr (0.96/0.80 mm) Micro catheter, GMA Co., Japan] using an oily marker pen (MO-120-MC-BK, Zebra, Japan) [see Figs. 6(a) and (c)]. The catheter was covered with a sheath and then inserted into a circulatory system made of acrylic resin [see Fig. 3(b)] and moved by hand slowly to validate its tracking ability, the motion being recorded by a digital camera (Canon PowerShot G10, Japan).

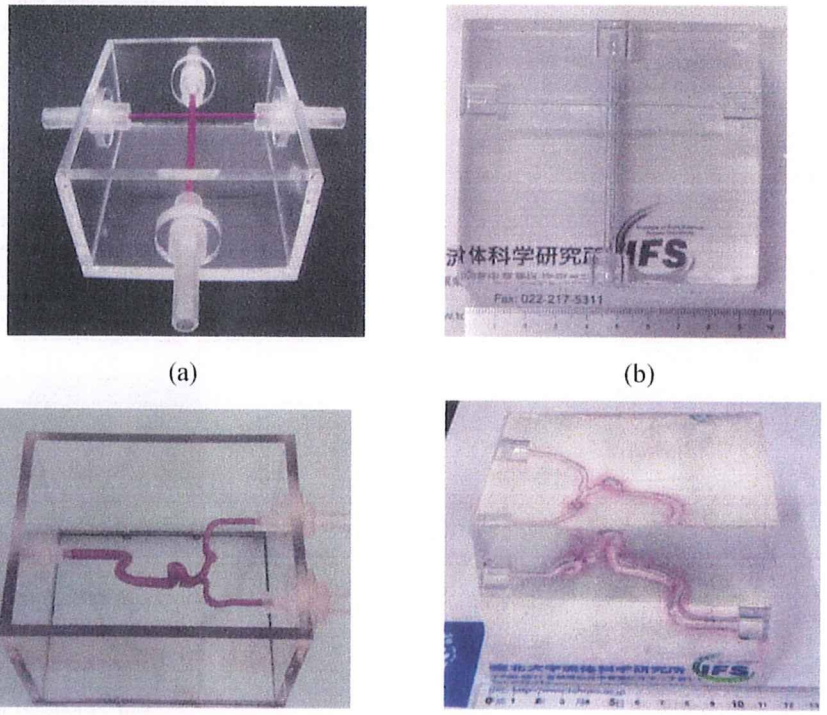

(a) (b)

(c) (d)

Fig. 2 Lost wax technique: (a) Acrylic resin with a cross geometry mold (b) Cross geometry of PVA-H model (c) Acrylic resin with a realistic geometry mold (d) Realistic geometry of PVA-H model

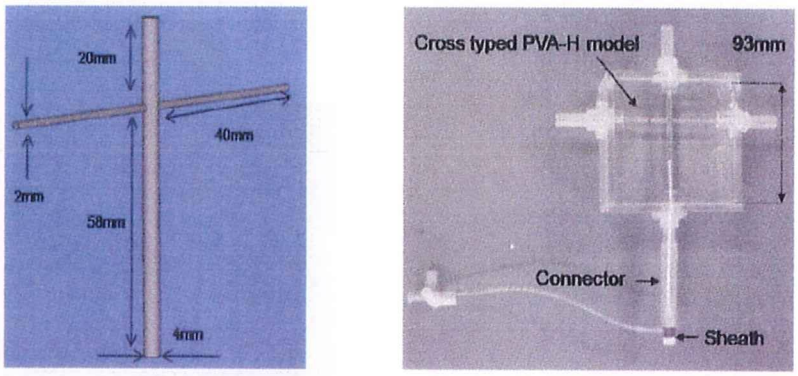

(a) (b)

Fig. 3 In vitro tracking system: (a) Cross mold for tracking system (b) Circulatory system for tracking motion of catheter

2.3. Realistic geometry of the PVA-H Model for Tracking System and Motion Capture of Catheter

To construct a realistic mold, models of the cerebral vasculature shown in Fig. 4 were created from patients undergoing clinically indicated conventional angiography with rotational data acquisition. Three-dimensional angiography was performed on a biplane C-arc unit (BV 3000; Philips Medical Systems, the Netherlands). The rotational run was then transferred to an angiography workstation (INTEGRIS 3D-RA, Philips Medical System) and 3-D reconstruction was performed. The 3-D geometry was transferred to a model made of gypsum, shown as Fig. 5. After gelation, the gypsum materials were removed by the lost-wax technique [14].

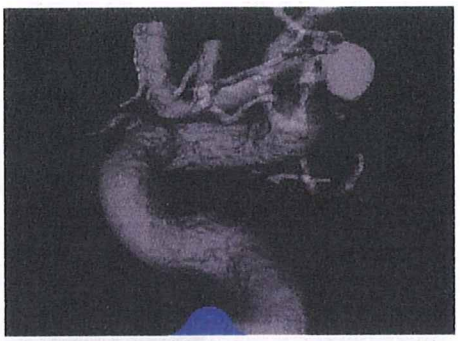

Fig. 4 Three-dimensional model for a patient

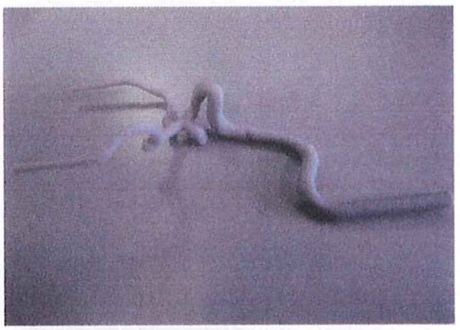

Fig. 5 Model made of gypsum

The circulatory system consists of a PVA-H model, an acrylic mold of that model, a sheath and a connecter, Two different parts of the catheter shown as Figs. 6(a) and (c), were inserted into the circulatory system and the motion was recorded by a digital camera.

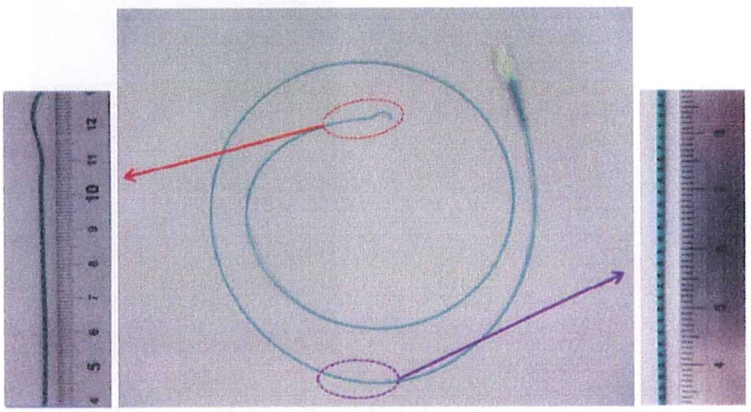

(a) (b) (c)

Fig. 6 Micro catheter made by GMA: (a) Soft part of catheter (b) 2.9/2.4 Fr (0.96/0.80 mm) (c) Hard part of catheter

3. Results

Figure 7 is a photograph of the catheter in the cross geometry of an artery. The catheter can be inserted into the artery smoothly. The cross geometry of the PVA-H model is sufficiently transparent to observe the catheter zebra patterns. The artery is soft and the catheter can be moved by hand force.

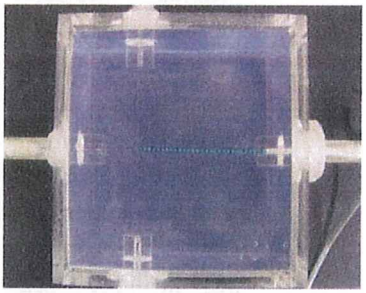

Fig.7 Micro catheter in PVA-H model with a cross geometry

Figure 8 shows consecutive images of catheter motion with time at the point of artery crossing. It demonstrates that the catheter tip in cross geometry of the PVA-H model can be gently moved so as to enter the horizontal artery, which implies that catheters and guidewires can be controlled in the actual PVA-H artery phantom model.

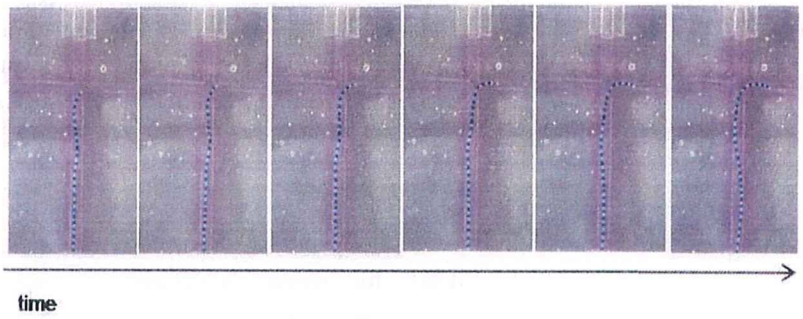

Fig. 8 Sequent images of catheter motion with time at the point of artery crossing

To assess the catheter's trackability, two different parts of the catheter, i.e., the hard part and the soft part, were inserted into the PVA-H model of the circulatory system with realistic geometry, as shown in Fig. 2(d). The soft part of the catheter [see Fig. 6(a)] can be controlled to gently move along the curved line of the PVA-H model with realistic geometry shown in Fig. 9. However, movement of the hard part [see Fig. 6(c)] was unsuccessful and we couldn't let catheter move on the curved line, which implies that more such experiments may lead to development of a good catheter using the in vitro tracking system for catheter motion.

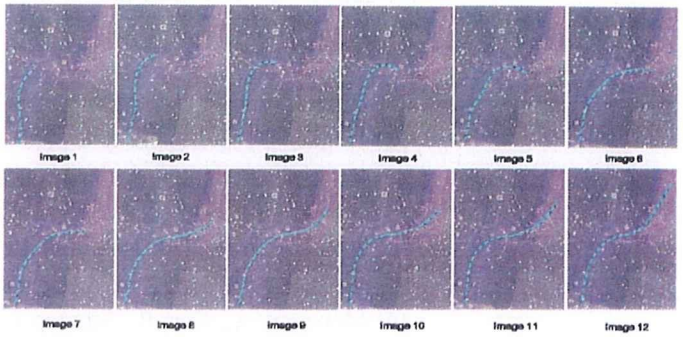

Fig. 9 Motion capture of the catheter with realistic geometry of PVA-H model

4. Discussion

Endovascular treatments using catheters have been applied for detection of aneurysms or stenosis for the past several decades. As the motion of the catheter is captured using a medical imaging system with x-ray, this treatment is termed IGMIT (Image Guided Minimally Invasive Treatment) [17]. The role of a catheter is to carry drugs and implants during surgery. However, the use of a catheter requires highly skilled operators and medical imaging systems can detect only the small markers on the catheter. To support the imaging, a navigator or a simulator has been developed for computer aided surgery [7], [8]. However, such systems only show results of the force interface between the operator and the system.

On the other hand, Takashima et al. have developed a computer-based simulator for catheter navigation for surgical planning based on force and balance in a catheter and an artery [9], [10]. This simulator would be useful for analysis of the structure of a catheter and may facilitate the design of a new catheter.

The clarity of PVA-H is sufficient to observe a catheter or a guide wire through the wall. Optical deformation of the catheter is observed at the edge of the PVA-H on the connector. The difference between the refraction of acrylic resin and that of PVA-H may cause this optical division at the edge. As a connector made of acrylic resin is necessary to fix a sheath to support the catheter, the edge must remain. As the refraction of PVA-H is also different from that of air, calibration should be performed for accurate measurement of the strain.

Because PVA-H contains water, its drying may limit measurement time to around 30 minutes. The humidity of PVA-H containing DMSO is maintained longer than that without DMSO. When a laser is used, care must be taken with regard to surface temperature because the melting point of PVA-H is around 70° C.

5. Conclusion

In this paper, we have described a study on the development of an in vitro tracking system for catheter movement by using a PVA-H model and evaluated the system by observation of filmed catheter motion. The transparency of PVA-H was sufficient for observation of the catheter through the PVA-H wall. PVA-H can be used to reconstruct the shape of an artery based on geometrical data of a patient. It also seems to be useful for medical doctors to receive training in catheter use and evaluation of catheter movement for endovascular treatment.

Acknowledgement

We acknowledge the support of Tohoku University Global COE Program "World Center of Education and Research for Trans-disciplinary Flow Dynamics" and partial support by a JSPS Core-to-Core Program grant, No. 20001.

References

(1) United Nations, *Demographic Yearbook 2004,* (2007), United Nations Publications.
(2) Schafer S., Hoffmann K.R., Noel P.B., Ionita C.N. and Dmochowski J., Evaluation of guidewire path reproducibility, *Med.Phys*, Vol. 35, No. 5 (2008), pp. 1884-1892.
(3) Ministry of Health, Labour and Welfare. "Statics and Other data : Press Release" available from< http://www.mhlw.go.jp/toukei/saikin/hw/jinkou/kakutei08/dl/01.pdf>, (accessed 2009-09-3).
(4) Molyneux A., Kerr R., Stratton I., Sandercock P., Clarke M., Shrimpton J. and Holman R., International subarachnoid aneurysm trial (ISAT) of neurosurgical clipping versus

endovascular coiling in 2143 patients with ruptured intracranial aneurysms: a randomised trial, *Lancet*, Vol. 360, No. 9342 (2002), pp. 1267-1274.

(5) Wiebers D. O., Whisnant J. P., Huston J., 3rd, Meissner I., Brown R. D., Jr., Piepgras D. G., Forbes G. S., Thielen K., Nichols D., O'Fallon W. M., Peacock J., Jaeger L., Kassell N. F., Kongable-Beckman G. L. and Torner J. C., Unruptured intracranial aneurysms: natural history, clinical outcome, and risks of surgical and endovascular treatment, *Lancet*, Vol. 362, No. 9378 (2003), pp. 103-110.

(6) Rufenacht D. A., Ohta M., Yilmaz H., Miranda C., Ruiz D. S., Abdo G. and Lylyk P., Current concept of endovascular aneurysm treatment and about the role of stents for endovascular repair of cerebral arteries, *Swiss Archives of Neurology and Psychiatry*, Vol. 348, No. 7 (2004), pp. 348-352.

(7) Tercero C., Okada Y., Ikeda S., Fukuda T., Sekiyama K., Negoro M. and Takahashi I., Numerical evaluation method for catheter prototypes using photo-elastic stress analysis on patient-specific vascular model, *Int J Med Robot*, Vol. 3 (2007), pp. 349-354.

(8) Tercero C., Ikeda S., Uchiyama T., Fukuda T., Arai F., Okada Y, Ono Y., Hattori R., Yamamoto T., Negoro M. and Takahashi I., Autonomous catheter insertion system using magnetic motion capture sensor for endovascular surgery, *Int J Med Robot*, Vol. 3 (2007), pp. 52-58.

(9) Takashima K., Ota S., Ohta M., Yoshinaka K. and Mukai T., Development of computer-based simulator for catheter navigation in blood vessels (2nd report, evaluation of torquability of guidewire), *Transactions of the Japan Society of Mechanical Engineers , Series* C, Vol. 73, No. 735 (2007), pp. 2988-2995. (in Japanese)

(10) Takashima K., Ota S., Ohta M., Yoshinaka K. and Mukai T., Development of a catheter and guideline simulator for interventional therapy, *Journal of Japanese Society of Biorheology (B&R)* Vol. 22, No.1 (2008), pp. 1-7. (in Japanese)

(11) Ohta M., Handa A., Iwata H., Rufenacht D. A. and Tsutsumi S., Poly-vinyl alcohol hydrogel vascular models for in vitro aneurysm simulations: the key to low friction surfaces, *Technology and Health Care*, Vol. 12 (2004), pp. 225-233.

(12) Kosukegawa H., Mamada K., Kuroki K., Liu L., Inoue K., Hayase T. and Ohta M., Measurements of dynamic viscoelasticity of Poly(vinyl alcohol) hydrogel for the development of blood vessel biomodeling, *Journal of Fluid Science and Technology*, 3-4(2008), pp. 533-543, (http://www.jstage.jst.go.jp/article/jfst/3/4/533/_pdf).

(13) Mamada K., Kosukegawa H., Yamaguchi K., Oikawa N., Katakura Y., Shibaya Y., Kuroki K. and Ohta M., Sensory evaluation of poly (vinyl alcohol) gel for surgical operation of soft tissue, *The 5th International Intracranial Stent Symposium*, No.P-23 (2008-5), pp. 26.

(14) Wetzel S.G., Ohta M., Handa A., Auer J.M., Lylyk P., Lovblad K.O., Babic D., and Rufenacht D.A., From patient to model: 3-D modeling of the cerebral vasculature based on rotational angiography, *AJNR Am J Neuroradiol* , Vol. 26, (2005), pp. 1425-1427.

(15) Ohta M., and Rufenacht D.A., Three-dimensional geometry measurements of cerebral aneurysms and vessel sizes for analytic geometry, *JSME, Fluid Engineering Conference 2006*, Vol. 06, No.21 (2006), pp. 355-356.

(16) Ohta M., Lachenal Y., Augsburger G., Abdo G., Yilmaz H., Fujimura N., Babic D., Lylyk P. and Rufenacht D.A., Three-dimensional measurements of cerebral aneurysms and vessel size, *Journal of Biomechanics* Vol. 39, S1 (2006), pp. S364.

(17) Rufenacht D.A., Ohta M., Yilmaz H., Miranda C., San Millan Ruiz D., Abdo G., and Lylyk P., Current concepts of endovascular aneurysm treatment, and the role of stents for endovascular repair of cerebral arteries, *Swiss Archives of Neurology and Psychiatry*, Vol. 155, No. 7 (2004), pp. 348-352.

ノート

キャピラリー電気泳動法による家庭用品塗膜の鉛溶出量調査

伊佐間和郎，河上強志，土屋利江，松岡厚子
国立医薬品食品衛生研究所

Capillary Electrophoresis Research into Lead Elution from Paint Films on Household Products

Kazuo ISAMA, Tsuyoshi KAWAKAMI, Toshie TSUCHIYA, Atsuko MATSUOKA
National Institute of Health Sciences: 1-18-1 Kamiyoga, Setagaya-ku, Tokyo 158-8501, Japan

Abstract

The Food Sanitation Law of Japan provides that the amount of lead eluted from the paint film on baby toys must be less than 90 μg/g. However, the amount of lead eluted from paint films on products to which the Food Sanitation Law is inapplicable is not controlled even if the product is used by babies. We therefore investigated the amount of lead eluted from the paint films on household products which babies may use with reference to the Food Sanitation Law. In addition, we confirmed the validity of capillary electrophoresis for measurement of the lead concentration of test solutions. Of 105 products (107 paint films) such as stationery and hairpins, only one hairpin had a paint film that eluted a small amount of lead. The hairpin package carried a warning of the lead content. Nevertheless, household product which babies may use should ideally not contain lead.

Keywords: capillary electrophoresis, lead, paint film, household product

Ⅰ．緒　言

鉛は中枢神経障害、腎機能障害、生殖機能障害及び造血器障害を生じる有害金属元素のひとつであり、特に、乳幼児に対しては、一定レベル以上の血中濃度で、知能や神経の発達に有害な影響を与える可能性がある[1, 2]。国際標準化機構（International Organization for Standardization、ISO）は、ISO 8124-3: 1997 Safety of toys – Part 3: Migration of certain elements を規定し、6歳以下の幼児用玩具を対象として、鉛の溶出限度値を90 mg/kg 玩具材料と定めている。また、我が国の食品衛生法は、飲食に起因する衛生上の危害の発生の防止を目的とするものであるが、乳幼児玩具には、乳幼児が口に接触することをその本質とするおもちゃが存在すること、及び一定年齢の乳幼児には、身の周りにあるものを口に入れるという性質があること等の理由から、同法に基づき、乳幼児が接触することによりその健康を損なうおそれがあるものとして厚生労働大臣が指定する玩具（指定おもちゃ）が規定され、また、同法に基づき、必要な規格及び製造基準が設定されている。平成20年3月31日に、食品衛生法に基づく「食品、添加物等の規格基準」の「おもちゃ又はその原材料の規格」が改正され、乳幼児用玩具の鉛等の規格について、国際的な整合性を考慮して、ISO 8124-3: 1997を採用する等規制が強化された[3-8]。しかしながら、食品衛生法に基づく指定おもちゃに該当しない、主として一般消費者の生活の用に供される製品（家庭用品）に含有する鉛は、今のところ規制されておらず、乳幼

〒158-8501　東京都世田谷区上用賀 1-18-1
E-mail: isama@nihs.go.jp